Bragg diffraction of spin waves from a two-dimensional antidot lattice

R. Zivieri,[1,*] S. Tacchi,[2] F. Montoncello,[1] L. Giovannini,[1] F. Nizzoli,[1] M. Madami,[2] G. Gubbiotti,[2,3] G. Carlotti,[2] S. Neusser,[4] G. Duerr,[4] and D. Grundler[4]

[1]*Consorzio Nazionale Interuniversitario per le Scienze Fisiche della Materia (CNISM) Unità di Ferrara and Dipartimento di Fisica, Università di Ferrara, Via Saragat 1, I-44122 Ferrara, Italy*

[2]*Consorzio Nazionale Interuniversitario per le Scienze Fisiche della Materia (CNISM) Unità di Perugia and Dipartimento di Fisica, Università di Perugia, Via A. Pascoli, I-06123 Perugia, Italy*

[3]*Istituto Officina dei Materiali del CNR (CNR-IOM), Unità di Perugia, c/o Dipartimento di Fisica, Via A. Pascoli, I-06123 Perugia, Italy*

[4]*Lehrstuhl für Physik funktionaler Schichtsysteme, Technische Universität München, Physik Department, James-Franck-Strasse 1, D-85747 Garching b. München, Germany*

(Received 16 December 2011; published 11 January 2012)

The spin-wave band structure of a two-dimensional square array of NiFe circular antidots (hole diameter 120 nm, periodicity 800 nm) is investigated. Brillouin light scattering experiments and band structure calculations, carried out by means of the dynamical matrix method, provide evidence for either extended or localized magnonic modes. Both families exhibit band gaps at Brillouin zone boundaries, attributed to Bragg reflection. Their calculated magnitude agrees with the one obtained by using an analytical model that takes into account the periodic variation of the internal field. This is in contrast to antidots in photonics and electronics, where the back-reflection is directly caused by the presence of holes. The results are important for advancing research on nanostructured two-dimensional magnonic crystals.

DOI: 10.1103/PhysRevB.85.012403 PACS number(s): 75.30.Ds, 75.78.Cd, 78.35.+c

Magnonic crystals (MCs) represent a new class of metamaterials with periodically modulated magnetic properties, where, similar to light in photonic crystals or electrons in artificial crystals, allowed frequency bands and ranges of forbidden gaps are present in the dispersion curves of spin excitations.[1,2] The first evidence for Bragg reflection of spin waves (SWs) and occurrence of a rejection band in one-dimensional (1D) MCs was given in stripes of periodical varying width.[3] Two-dimensional (2D) MCs can be realized in the form of a periodic array of interacting nanomagnets (dots)[4,5] or holes in a ferromagnetic film (i.e., antidot [AD] array).[6] In this respect, propagation of SWs in AD lattices, consisting of 2D periodic arrays of nanopatterned holes etched into a continuous ferromagnetic film, has been extensively investigated in the last years because of the possibility to control SW propagation on the nanoscale.[7,8] In order to interpret the frequency dispersion of the propagating SWs in 2D AD, an analytical model, based on the theory of propagating SWs in transversely magnetized stripes with effective width equal to the neighboring holes distance, has been proposed.[7,9] However, this model cannot account for the presence of magnonic bands and band gaps, the understanding of which is a key point from a fundamental perspective, but also for its potential technological applications. MCs are in fact promising to realize new SW-based devices, such as filters, waveguides, and magnonic logic circuits, operating in the GHz frequency range.[10] Since the wavelengths of spin waves are shorter than those of electromagnetic radiation in the GHz range, dimensions of MCs devices can be scaled down by several orders of magnitude with respect to photonic devices, with the advantage that dispersion characteristics are tunable by variation of the bias magnetic field.

In this Brief Report, we provide the first experimental evidence together with the first theoretical systematic investigation for opening of magnonic band gaps in 2D AD lattice. Opening of band gaps is interpreted in terms of Bragg diffraction of SWs from the AD lattice, and a quantitative explanation of this effect is given by studying the behavior of the internal field. The mode frequencies were measured by means of Brillouin light scattering (BLS), while band structure was calculated by using the dynamical matrix method (DMM) with implemented periodic boundary conditions (PBC) and band gaps estimated by an analytical approach. We emphasize that the discussion of bands and band gaps given for this geometry can be considered general and also applied to different AD geometries of submicrometric size and magnetic materials in a saturated magnetic ground state.

A 22-nm-thick Permalloy ($Ni_{80}Fe_{20}$, Py) film was periodically patterned using focused ion-beam into a square lattice with holes of diameter $\delta = 120 \pm 30$ nm, forming an AD array of periodicity $a = 800$ nm.[7] A scanning electron microscope image of the sample is shown as an inset in Fig. 1. BLS spectra are recorded in the backscattering configuration by using a Sandercock-type high-contrast and high-resolution $(3 + 3)$ tandem Fabry-Pérot interferometer in the Damon-Eshbach scattering geometry, where the wave vector $\boldsymbol{q}$ is perpendicular to $\boldsymbol{H}$. The laser wavelength is $\lambda = 532$ nm. In order to change the magnitude of the wave vector $\boldsymbol{q}$, the incidence angle of light θ is varied. This angle is linked to $\boldsymbol{q}$ by the relation $q = (4\pi/\lambda)\sin\theta$. In this Brief Report, we explore wave vectors up to 2.2×10^5 rad/cm, which corresponds to the reciprocal space up to the sixth Brillouin zone (BZ). A magnetic field of magnitude $H = 200$ Oe, sufficient to saturate the sample, is applied in the sample plane along the y-axis.

The equilibrium magnetization state, in the presence of such an applied magnetic field, is calculated with a micromagnetic code by using typical Py magnetic parameters: $4\pi M_s = 9.4$ kG, $\gamma/2\pi = 2.95$ GHz/kOe, and $A = 1.3 \times 10^{-6}$ erg/cm, where M_s is the saturation magnetization, γ is the gyromagnetic ratio, and A is the exchange stiffness constant. With these

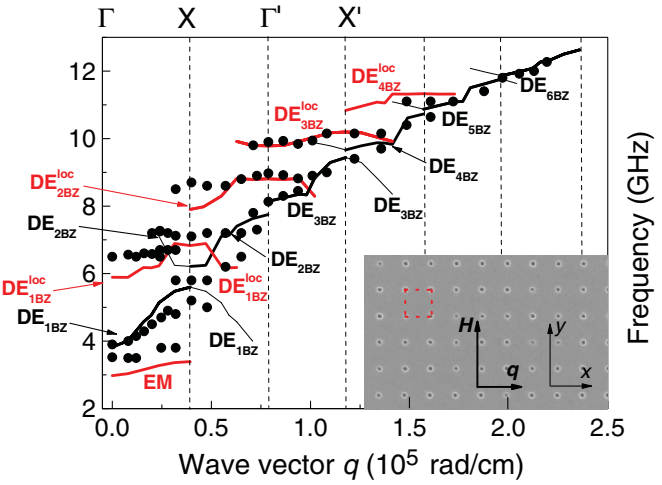

FIG. 1. (Color online) Experimental BLS data (full circles) and calculated bands (full lines). The thick black curve in the subsequent BZs represents the main propagating mode of the system. The thin black curves are replicas of this mode in adjacent BZs. The red/dark gray curves represent other modes as described in the text. The dashed vertical lines mark the borders between adjacent BZs. Inset: scanning electron microscopy image of the periodic array of holes in Py showing the directions of $\boldsymbol{H}$ and $\boldsymbol{q}$. The rectangular area (dashed red lines) indicates the primitive cell.

parameters, the exchange length is $l_{\text{exch}} = \sqrt{A/2\pi M_s^2} \cong 6$nm. Hence, we subdivide the sample into cells (parallelepipeds) having size $\Delta_x \times \Delta_y \times \Delta_z = 5$ nm $\times$ 5 nm $\times$ 22 nm with a total of 25,152 active micromagnetic cells in the primitive cell (supercell) shown in the inset of Fig. 1. Due to the presence of holes, the distribution of the ground-state magnetization is non-collinear and exhibits small deviations from the direction of $\boldsymbol{H}$ close to the ADs. In the calculations, we assume the dynamic magnetization $\delta\boldsymbol{m}_{\boldsymbol{K}}(\boldsymbol{r})$ to take the Bloch wave form, namely, $\delta\boldsymbol{m}_{\boldsymbol{K}}(\boldsymbol{r}) = \delta\tilde{\boldsymbol{m}}_{\boldsymbol{K}}(\boldsymbol{r})e^{i\boldsymbol{K}\cdot\boldsymbol{r}}$, where $\boldsymbol{K}$ is the Bloch wave vector, and $\delta\tilde{\boldsymbol{m}}_{\boldsymbol{K}}(\boldsymbol{r})$ is the periodic dynamic magnetization, which represents the solution, for a particular wave vector $\boldsymbol{K}$ and a given mode, of the DMM eigenvalue problem within the primitive cell.

In extended magnetic systems like AD arrays studied by DMM with PBC, in addition to the usual nearest-neighbors exchange interaction between micromagnetic cells,[11] the exchange contribution across nearest-neighbors micromagnetic cells belonging to adjacent surface supercells must be taken into account. Hence, the exchange energy density of the given supercell takes the form

$$E_{\text{ex}} = A \sum_i \sum_l \frac{(1 - \boldsymbol{m}_i \cdot \boldsymbol{m}_l)}{a_{il}^2}, \qquad (1)$$

where $\boldsymbol{m}_i = \frac{\boldsymbol{M}_i}{M_s}$ ($\boldsymbol{m}_l = \frac{\boldsymbol{M}_l}{M_s}$) is the reduced magnetization in the ith (lth) cell. The first sum (index i) runs over all the micromagnetic cells of the supercell; the second sum (index l) runs over the nearest-neighbors of the ith micromagnetic cell. The variable a_{il} is the distance between the centers of two adjacent cells of indices i and l, respectively. When the ith micromagnetic cell is on one of the edges (vertices) of the given supercell, the interaction with one (two) micromagnetic cell(s) belonging to the correct nearest supercell must be added.

Figure 1 shows the measured spin-wave frequencies as a function of the transferred wave vector, together with the calculated dispersion curves. BLS spectra consist of series of discrete peaks, which merge into one for wave vectors larger than 1.5×10^5 rad/cm. It can be seen that some of the observed modes exhibit a marked dispersive character, while other modes have a prevalent stationary behavior, characterized by an almost constant frequency. According to our calculations, the detected spin-wave modes can be classified by taking into account the features of their spatial extension along the x direction indicated in the inset of Fig. 1. Based on this observation, we reduce the problem, in a first approximation, to an effective 1D problem by singling out the dependence on the Bloch wave vector (along x) and neglecting the less pronounced oscillation along the y direction. Our model might thus apply also to the Py waveguide of modulating width considered in Ref. 3. Within such an approximation, as illustrated in Fig. 2, two distinct families of propagating modes can be recognized:

(1) *Extended modes* spreading in the horizontal "channels" (along the x direction, parallel to $\boldsymbol{q}$) exist between adjacent rows of holes but have a non-vanishing amplitude along the horizontal rows of holes. These modes are dispersive and are analogous to the extended surface Damon-Eshbach (DE) mode of a continuous film.[12] However, in this case, a band gap appears at each BZ boundary both in measurements and calculations, so that we label the mode with the largest calculated cross section in the nth BZ as $\text{DE}_{n\text{BZ}}$, where $n =$ 1,2,..., and it takes the role of a "band index." At the center of the first Brillouin zone (1BZ) ($q \approx 0$), the $\text{DE}_{1\text{BZ}}$ mode corresponds to the uniform precessional mode (Kittel mode), the spatial profile of which has been measured.[7]

The frequencies of the calculated modes are shown in the extended zone scheme, which refers to the transferred wave vector $\boldsymbol{q} = \boldsymbol{K}$. For a few modes, the dispersion curves are also repeated in neighboring BZs in order to mark the normal modes of large calculated scattering cross sections. The overall agreement between results of micromagnetic calculations and BLS measurements is very good apart from an overestimation of the measured frequencies in the vicinity of $K = \pi/a$. In particular, the calculated band gap at the border of the 1BZ ($K = \pi/a$) between the $\text{DE}_{1\text{BZ}}$ and the $\text{DE}_{2\text{BZ}}$ band turns out to be 0.6 GHz and is in excellent agreement with the measured one. The band gap between the $\text{DE}_{n\text{BZ}}$ modes decreases with increasing n and eventually vanishes for large values of n. The physical reason underlying the appearance of band gaps at BZ boundaries is due to the different spatial localization of the dynamic magnetization as shown in Fig. 2. For example, at the edge of the 1BZ, the group velocity of both the upper ($\text{DE}_{2\text{BZ}}$) and the lower ($\text{DE}_{1\text{BZ}}$) modes vanishes, and these modes behave as two stationary waves, which differ by a spatial shift of a quarter of the wavelength. In particular, the amplitude of the lowest-frequency mode ($\text{DE}_{1\text{BZ}}$) has its maxima between vertical rows of holes in Fig. 2(a). In the horizontal channels, the spin precession amplitude is proportional to $\sin(\pi/a)\,x$. The $\text{DE}_{2\text{BZ}}$ mode has its largest amplitude in between the holes in vertical direction and takes a form proportional to $\cos(\pi/a)\,x$ in the horizontal direction.

(2) *Localized modes* are mainly concentrated along the horizontal rows of holes (Figs. 2(b) to 2(d)). These modes

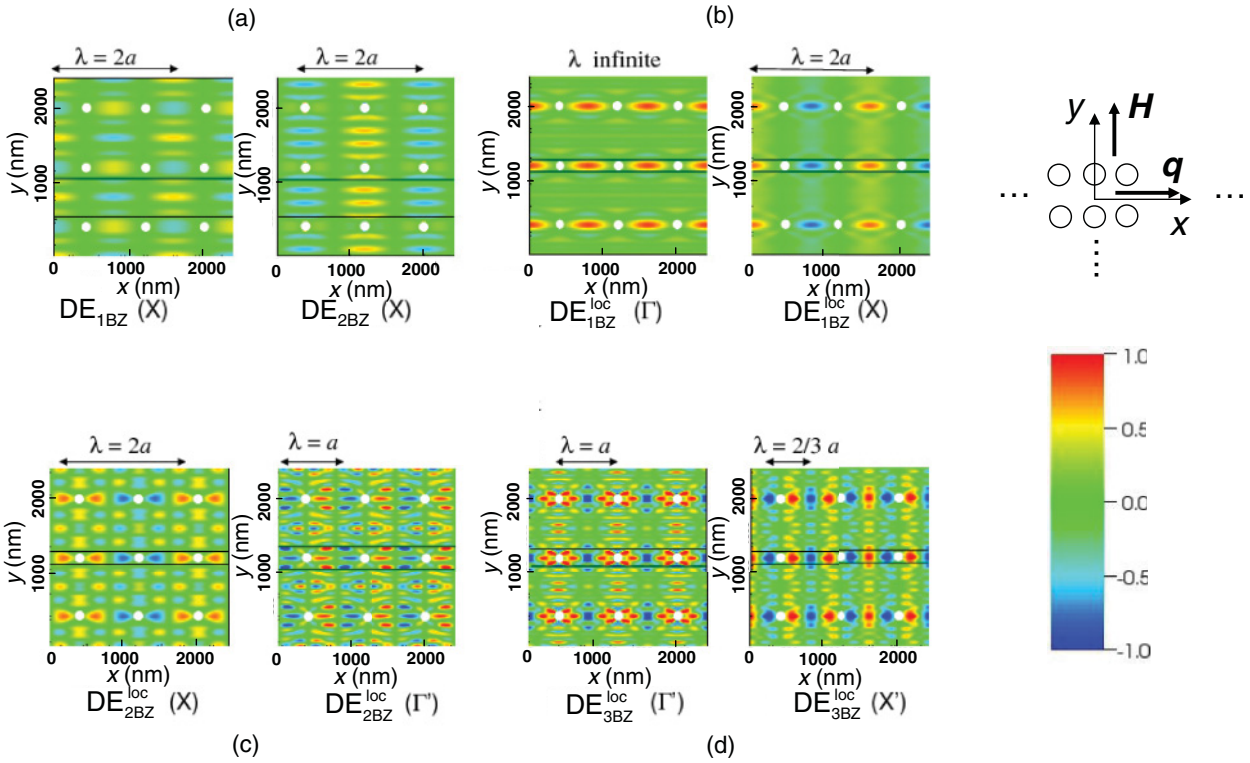

FIG. 2. (Color online) Calculated spatial profiles of representative modes in 3 × 3 primitive cells. The real part of the out-of-plane component of the dynamic magnetization is plotted. For each mode, regions of large precession amplitudes are indicated. The corresponding wavelengths at different high-symmetry points are also shown. A reference frame with the directions of $\boldsymbol{H}$ and $\boldsymbol{q}$ is also shown.

exhibit a pronounced localized spatial profile[13] and resemble the weak dispersive resonances observed in chains of magnetic dots.[14] They are therefore labeled as $\mathrm{DE}^{\mathrm{loc}}_{n\,\mathrm{BZ}}$ modes, where the label "loc" emphasizes their localized character along rows of ADs. The dispersion of these modes is less pronounced if compared to those observed for the extended modes, due to the spatial localization. Note that in such a case, the agreement between the measured and the calculated frequency bandwidth (BW) is quite good, except for the lowest bands of localized modes. This discrepancy is attributed to possible variation of the hole diameters in the real AD.

Eventually, in addition to the aforementioned families of extended and localized modes, we find, at very low frequency, the so-called edge mode (EM).[15] This mode exhibits a weakly dispersive behavior, due to its strong spatial localization in the regions adjacent to edges of ADs, where the internal field is highly inhomogeneous. The calculated band has a width of about 0.4 GHz and is slightly downshifted with respect to the experimental data. This difference is ascribed to the presence of imperfections at the border of the holes or to its imprecise discretization in the used model, which strongly affect the frequency of the EM.

As a final step of our investigation, we developed an analytical model to estimate the band gaps, in analogy to the well-known case of Bragg reflection of electrons in a periodic potential.[16] To achieve this goal, we first estimate the mean internal field acting on precessing spins via $\langle H^y_{\mathrm{int}}(x)\rangle = \frac{1}{N_y}\sum_{N_y} H^y_{\mathrm{int}}(x,y)$ by averaging over a relevant number N_y of micromagnetic cells along y direction using the OOMMF micromagnetic code.[17] In particular, $H^y_{\mathrm{int}}(x,y) = H + H^y_{\mathrm{dem}}(x,y)$, where H^y_{dem} is the y-component of the demagnetizing field $\boldsymbol{H}_{\mathbf{dem}}$. Note that the contribution of the static exchange field is negligible. (To reproduce the internal field of the periodic system in a realistic way, we have simulated a 5 × 5 AD system, corresponding to 664 × 664 micromagnetic cells.)

The mean internal field $\langle H^{y\ \mathrm{extended}}_{\mathrm{int}}(x)\rangle$ experienced by extended modes is estimated by averaging over the total number of micromagnetic cells of the primitive cell along the y direction (Fig. 3). For localized modes, instead, the average $\langle H^{y\ \mathrm{loc}}_{\mathrm{int}}(x)\rangle$ is performed over 28 cells in the y direction, corresponding to their region of localization at the border of BZs (Fig. 3). As it can be seen in Figs. 3(a) and 3(c), both $\langle H^{y\ \mathrm{extended}}_{\mathrm{int}}(x)\rangle$ and $\langle H^{y\ \mathrm{loc}}_{\mathrm{int}}(x)\rangle$, respectively, have periodical oscillations with maxima corresponding to the hole lattice. As illustrated in Fig. 3(e), in fact, $\boldsymbol{H}_{\mathbf{dem}}$ inside the holes is aligned with $\boldsymbol{H}$ due to the opposite uncompensated distribution of surface "magnetic charges" in the holes with respect to that of the magnetic material in which the holes are embedded.

In order to derive a simple analytical formula for band gaps showing the role of the internal field for opening of band gaps, it is reasonable to describe approximately the mean internal fields $\langle H^{y\ \mathrm{extended}}_{\mathrm{int}}(x)\rangle$ and $\langle H^{y\ \mathrm{loc}}_{\mathrm{int}}(x)\rangle$ by a periodic rectangular function, which is maximum in correspondence with ADs (region 1 [1]: $-\frac{\delta}{2} + n_1 a \leqslant x \leqslant \frac{\delta}{2} + n_1 a$) and minimum between the ADs (region 2 [2]: $n_1 a + \frac{\delta}{2} \leqslant x \leqslant [n_1 + 1]\,a - \frac{\delta}{2}$) with $n_1 = 0, \pm 1, \pm 2, \ldots$. Therefore, $\langle H^{y\ (1)i}_{\mathrm{int}}\rangle =$

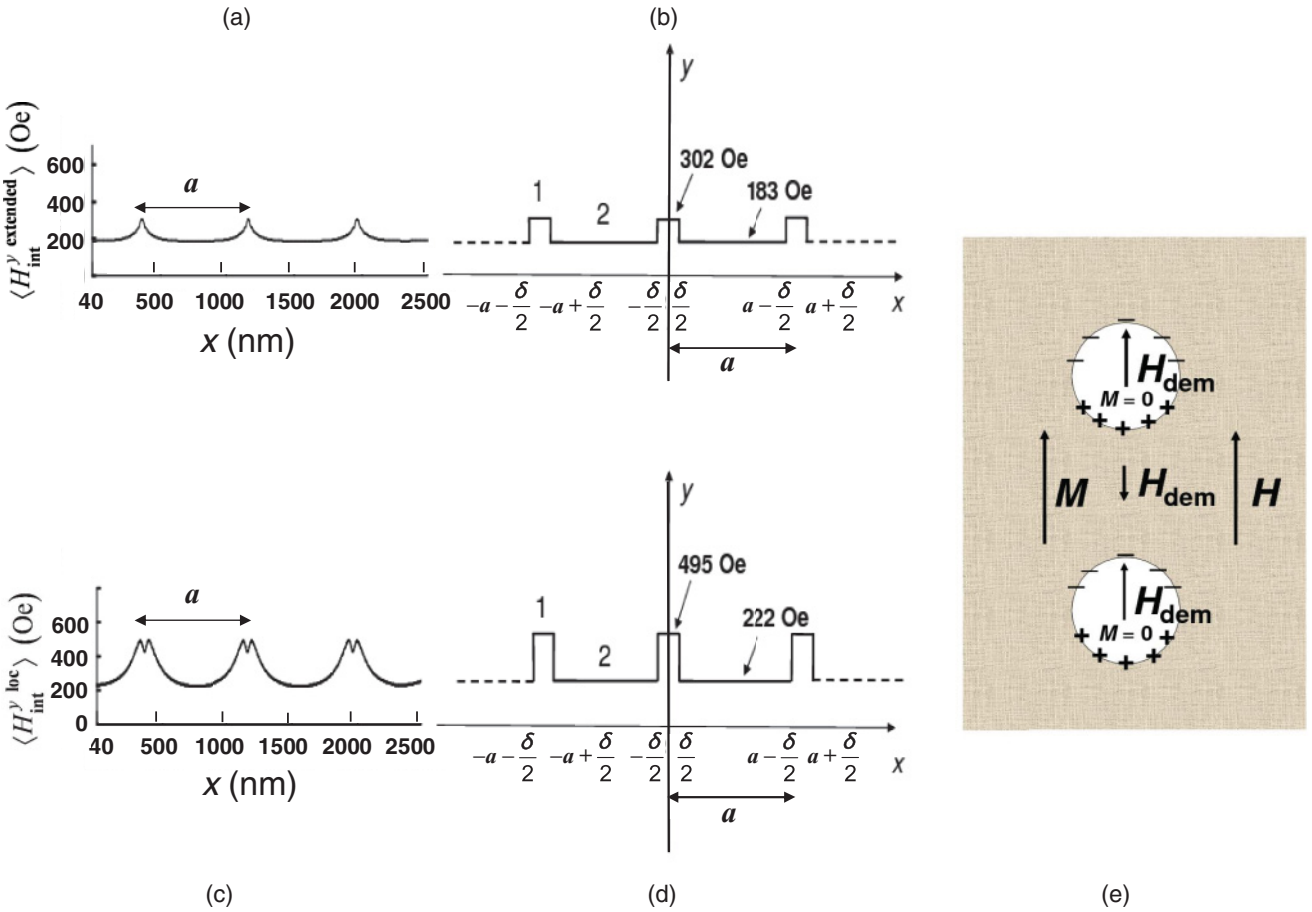

FIG. 3. (Color online) (a) Periodic mean internal field along the x direction relevant for spin-wave modes of Fig. 2(a) extending through the channels. (b) Corresponding periodic rectangular function. The values of the internal field indicated by the arrows in regions 1 and 2 are extrapolated from the maxima and minima of the profile shown in panel (a). (c) Mean internal field relevant for spin-wave modes of Fig. 2(b) to (d) localized along rows of holes. (d) Approximation of (c) using a rectangular function. (e) Sketch of the AD lattice with two holes (white) embedded in the ferromagnetic film (dark). The orientations of $\boldsymbol{H}_{\mathbf{dem}}$, $\boldsymbol{H}$, and $\boldsymbol{M}$ together with the induced surface "magnetic charges" are shown.

$H + \langle H_{\mathrm{dem}}^{y\,(1)i}\rangle$ ($\langle H_{\mathrm{int}}^{y\,(2)i}\rangle = H + \langle H_{\mathrm{dem}}^{y\,(2)i}\rangle$) ($i =$ extended, loc), and values of the mean internal field are obtained by the OOMMF simulations and assumed constant in each of the two regions [Fig. 3(b)–3(d)]. Since we are dealing with a periodic system, the mean internal field can be expressed as a Fourier expansion over the reciprocal lattice vectors, namely $\langle H_{\mathrm{int}}^{y}(x)\rangle = \frac{H_{\mathrm{int}}^{0}}{2} + \sum_{k=1}^{\infty} H_{\mathrm{int}}^{k} \cos\frac{2k\pi}{a}x$, where H_{int}^{k} is the kth Fourier component, and $k = 1,2,\ldots$ (the superscript y is omitted on the right-hand side). It can be shown that the band splitting between a given couple of modes or band gap is proportional to the k-Fourier component of $\langle H_{\mathrm{int}}^{y}(x)\rangle$, viz.

$$H_{\mathrm{int}}^{k} = \frac{2}{a}\int_{-\frac{a}{2}}^{\frac{a}{2}} \left\langle H_{\mathrm{int}}^{y}(x)\right\rangle \cos\frac{2k\,\pi\,x}{a}dx. \qquad (2)$$

If compared to the dynamic exchange and dipolar fields, the difference of the mean internal field experienced by spin modes between the two regions can be considered as a small perturbation. Hence, we get according to perturbation theory

$$\Delta\nu^{k\,i} \approx \gamma/2\pi\left(2\left|H_{\mathrm{int}}^{k\,i}\right| M_s\right)^{1/2}, \qquad (3)$$

with

$$H_{\mathrm{int}}^{k\,i} = \frac{2}{k\pi}\left(\left\langle H_{\mathrm{int}}^{y(1)i}\right\rangle - \left\langle H_{\mathrm{int}}^{y\,(2)\,i}\right\rangle\right)\sin\frac{k\pi\,\delta}{a},\ \ i = \text{extended, loc.} \qquad (4)$$

In Eq. (3), $\Delta\nu^{k\,i} = \nu_{n+1}^{k\,i} - \nu_{n}^{k\,i}$ is the frequency splitting at the border of BZs with $n = 1,2,\ldots$. The $\mathrm{DE}_{2\mathrm{BZ}}$ mode exhibits its maximum precession amplitude in region 1, where $\langle H_{\mathrm{int}}^{y\ \mathrm{extended}}\rangle$ is larger and has thus a larger frequency. Instead, the maximum precession amplitude of the $\mathrm{DE}_{1\mathrm{BZ}}$ mode is in region 2, where $\langle H_{\mathrm{int}}^{y\ \mathrm{extended}}\rangle$ is smaller, and the mode has thus the smaller frequency. Similar features are found also for the $\mathrm{DE}_{2\,\mathrm{BZ}}^{\mathrm{loc}}$ and $\mathrm{DE}_{1\,\mathrm{BZ}}^{\mathrm{loc}}$ modes. A comparison between the band gap measured by BLS and the values calculated according to Eqs. (3) and (4) and by means of DMM is shown in Table I. The overall agreement is very good apart from an underestimation of the BLS observed band gap between the $\mathrm{DE}_{2\,\mathrm{BZ}}^{\mathrm{loc}}$ and $\mathrm{DE}_{1\,\mathrm{BZ}}^{\mathrm{loc}}$ modes, extracted from both analytical and DMM calculations. Band splitting vanishes, as expected, in the continuous film limit, namely for $\frac{\delta}{a} \to 0$. Fourier coefficients H_{int}^{ki} decrease with increasing k, leading to the narrowing of higher-order

TABLE I. Frequency band gaps calculated either at the border of the 1BZ ($k = 1$) or at the border of the 2BZ ($k = 2$) for the most representative spin modes. Each couple of modes is indicated in parentheses. The corresponding observed BLS frequency band gaps are also shown.

$\Delta\nu^k$ (GHz)	DMM	Analytical	BLS
$\Delta\nu^1$ ($DE_{2BZ} \div DE_{1BZ}$)	0.60	0.67	0.6
$\Delta\nu^1$ ($DE^{loc}_{2BZ} \div DE^{loc}_{1BZ}$)	1.01	1.11	1.6
$\Delta\nu^2$ ($DE^{loc}_{3BZ} \div DE^{loc}_{2BZ}$)	0.98	0.96	0.9

band gaps and confirming the trend found by means of DMM calculations.[18]

From the previous analytical description, it is clear that the occurrence of band gaps at the BZ boundaries can be interpreted as due to the Bragg diffraction for propagating SWs, because of the presence of the artificial periodicity of the internal field, which gives rise to a counterpropagating "Bragg-reflected" wave. However, it is important to notice that, according to Eqs. (3) and (4), the relevant scattering potential for Bragg reflection is not provided by the holes themselves, but by the concomitant internal field inhomogeneity *between* holes.

The main outcome of our model is consistent with Bragg reflection effects studied on an individual magnonic waveguide in Ref. 3, where the width was modulated periodically. There, the observed spin-wave rejection frequency band has been attributed to both internal field inhomogeneities and periodic confinement effects in the transverse direction due to the narrow stripe regions. To quantify the band gaps in our model, we consider only the field inhomogeneity and not the confinement. The 2D architecture of the nanopatterned antidot lattice has already been shown to support coherent coupling of unit cells in the transverse direction, counteracting confinement effects.[19]

Bragg reflection due to inhomogeneities between holes is fundamentally different from the case of Bragg reflection of light and electrons in corresponding AD lattices and artificial crystals.[20,21] Finally, it is interesting to note that the eigenfunctions representing frequency modes at the BZs boundaries belonging to nth and $(n + 1)$th band (sin $[k\pi/a]$ x and cos $[k\pi/a]$ x, with $k = 1,2,\ldots,$ respectively) are interchanged with respect to those of electrons in electronic bands studied within the nearly free electron model. This can be understood taking into account that the periodic mean internal field has its maxima in correspondence with ADs, while the periodic electronic potential is minimum close to the nuclei and vice versa. Moreover, also the BWs behavior vs the Bloch wave vector is opposite with respect to the electronic case for the range of wave vectors explored in the measurements: BWs in magnonic AD lattice decrease with increasing Bloch wave vector, while electronic BWs increase.

In conclusion, the band structure of collective modes for a 2D magnetic array of ADs was determined by using a micromagnetic approach, achieving a very good agreement with BLS experimental results. It has been shown that, in addition to extended modes propagating along channels of ADs, there exists another kind of back-reflected propagating modes mostly localized along rows of ADs. Band gaps are interpreted in terms of Bragg reflection according to an analytical model. To this respect, AD behaves not only as waveguide for SWs, but the presence of band gaps permits the frequency of traveling excitations to be filtered.

The research leading to these results has received funding from the European Community's Seventh Framework Programme (FP7/2007-2013) under Grant Agreement No. 228673 (MAGNONICS) and under Grant Agreement No. 233552 (DYNAMAG).

*zivieri@fe.infn.it

[1] J. O. Vasseur, L. Dobrzynski, B. Djafari-Rouhani, and H. Puszkarski, Phys. Rev. B **54**, 1043 (1996).
[2] A. V. Chumak, T. Neumann, A. A. Serga, B. Hillebrands, and M. P. Kostylev, J. Phys. D: Appl. Phys. **42**, 205005 (2009).
[3] A. V. Chumak, P. Pirro, A. A. Serga, M. P. Kostylev, R. L. Stamps, H. Schultheiss, K. Vogt, S. J. Hermsdoerfer, B. Laegel, P. A. Beck, and B. Hillebrands, Appl. Phys. Lett. **95**, 262508 (2009).
[4] S. Tacchi, F. Montoncello, M. Madami, G. Gubbiotti, G. Carlotti, L. Giovannini, R. Zivieri, F. Nizzoli, S. Jain, A. O. Adeyeye, and N. Singh, Phys. Rev. Lett. **107**, 127204 (2011).
[5] V. V. Kruglyak, P. S. Keatley, A. Neudert, R. J. Hicken, J. R. Childress, and J. A. Katine, Phys. Rev. Lett. **104**, 027201 (2010).
[6] S. L. Vysotskiĭ, S. A. Nikitov, and Yu. A. Filimonov, J. Exp. Theor. Phys. **101**, 547 (2005).
[7] S. Neusser, G. Duerr, H. G. Bauer, S. Tacchi, M. Madami, G. Woltersdorf, G. Gubbiotti, C. H. Back, and D. Grundler, Phys. Rev. Lett. **105**, 067208 (2010).
[8] H. Ulrichs, B. Lenk, and M. Münzenberg, Appl. Phys. Lett. **97**, 092506 (2010).
[9] M. Kostylev, G. Gubbiotti, G. Carlotti, G. Socino, S. Tacchi, C. Wang, N. Singh, A. O. Adeyeye, and R. L. Stamps, J. Appl. Phys. **103**, 07C507 (2008).
[10] A. B. Ustinov, A. V. Drozdovskii, and B. A. Kalinikos, Appl. Phys. Lett. **96**, 142513 (2010).
[11] L. Giovannini, F. Montoncello, and F. Nizzoli, Phys. Rev. B **75**, 024416 (2007).
[12] R. W. Damon and J. R. Eshbach, J. Phys. Chem. Solids **19**, 308 (1961).
[13] S. Tacchi, M. Madami, G. Gubbiotti, G. Carlotti, A. O. Adeyeye, S. Neusser, B. Botters, and D. Grundler, IEEE Trans. Magn. **46**, 172 (2010).
[14] R. Zivieri, F. Montoncello, L. Giovannini, F. Nizzoli, S. Tacchi, M. Madami, G. Gubbiotti, G. Carlotti, and A. O. Adeyeye, Phys. Rev. B **83**, 054431 (2011).
[15] S. Neusser, B. Botters, and D. Grundler, Phys. Rev. B **78**, 054406 (2008).

[16]C. Kittel, *Introduction to Solid State Physics*, 7th ed. (John Wiley & Sons, Inc., NY, 1996), p. 176.

[17]M. J. Donahue and D. G. Porter, *OOMMF User's Guide* (NIST, Gaithersburg, MD).

[18]Fourier coefficients H_{int}^{ki} determined numerically by Fourier transforming the mean internal fields shown in Fig. 3(a) and 3(c) differ slightly with respect to the approximated ones calculated according to Eq. (4).

[19]S. Neusser, H. G. Bauer, G. Duerr, R. Huber, S. Mamica, G. Woltersdorf, M. Krawczyk, C. H. Back, and D. Grundler, Phys. Rev. B **84**, 184411 (2011).

[20]J. D. Joannopoulos, S. G. Johnson, J. N. Winn, and R. D. Meade, *Photonic Crystals: Molding the Flow of Light*, 2nd ed. (Princeton University Press, Princeton, NJ, 2008).

[21]C. Flindt, N. A. Mortensen, and A.-P. Jauho, Nano Lett. **5**, 2515 (2005).